Studies of carbon monoxide release from ruthenium(II) bipyridine carbonyl complexes upon UV light exposure

Kubeil, M.; Vernooij, R. R.; Kubeil, C.; Wood, B. R.; Graham, B.; Stephan, H.; Spiccia, L.;

Originally published:

May 2017

Inorganic Chemistry 56(2017)10, 5941-5952

DOI: https://doi.org/10.1021/acs.inorgchem.7b00599

Studies of carbon monoxide release from ruthenium(II) bipyridine carbonyl complexes upon UV light exposure

Manja Kubeil†‖, Robbin R. Vernooij†§ǂ, Clemens Kubeil†, Bayden R. Wood†§, Bim Graham‡, Holger Stephan‖, and Leone Spiccia†*

† School of Chemistry, Monash University, Clayton, Victoria 3800, Australia

‖ Institute of Radiopharmaceutical Cancer Research, Helmholtz - Zentrum Dresden - Rossendorf, Bautzner Landstraße 400, D-01328, Dresden, Germany

§ Centre for Biospectroscopy, Monash University, Clayton, Victoria 3800, Australia

ǂ Department of Chemistry, University of Warwick, Gibbet Hill Road, Conventry CV4 7AL, U.K.

‡ Medicinal Chemistry, Monash Institute of Pharmaceutical Sciences, Monash University, Parkville, Victoria 3052, Australia

KEYWORDS

photoCORMs, ruthenium bipyridine carbonyl complexes, mechanism, TD-DFT, MCR-ALS

DEDICATION

Dedicated to our friend, mentor and colleague, Professor Leone Spiccia who passed away on 18th December 2016.

ABSTRACT

The UV light-induced CO release characteristics of a series of ruthenium(II) carbonyl complexes of the form trans-(Cl) [$RuLCl_2(CO)_2$] (L = 4,4'-dimethyl-2,2'-bipyridine, 4'-methyl-2,2'-bipyridine-4-carboxylic acid or 4,4'-dicarboxylic acid-2,2'-bipyridine) have been elucidated using a combination of UV-Vis absorbance and Fourier transform infrared (FTIR) spectroscopies, multivariate curve resolution-alternating least squares (MCR-ALS) analysis, and density functional theory calculations. In acetonitrile, photolysis appears to proceed via a serial three-step mechanism involving sequential formation of [$RuL(CO)(CH_3CN)Cl_2$], [$RuL(CH_3CN)_2Cl_2$], and [$RuL(CH_3CN)_3Cl]^+$. Release of the first CO molecule occurs quickly (k_1 >> 3 min^{-1}), while release of the second CO proceeds at a much more modest rate (k_2 = 0.099–0.17 min^{-1}) and is slowed by the presence of electron-withdrawing carboxyl substituents on the bipyridine ligand. In aqueous media (1% DMSO in H_2O), the two photo-decarbonylation steps proceed much more slowly (k_1 = 0.46–1.3 min^{-1} and k_2 = 0.026–0.035 min^{-1}, respectively) and the influence of the carboxyl groups is less pronounced. These results have implications for the design of new light-responsive CO-releasing molecules ("photoCORMs") intended for future medical use.

INTRODUCTION

Carbon monoxide-releasing molecules (CORMs)[1] represent a promising prodrug approach for the safe storage and controlled release of CO,[2-4] a molecule that has been shown to have a number of potentially useful therapeutic effects when administered in appropriate doses, including anti-inflammatory, vasodilatory and anti-microbial properties.[5-8] Most of the reported CORMs are group 7 and 8 transition metal carbonyl complexes.[5, 9-13] When in a low oxidation state, these complexes are stabilized by a synergistic combination of σ bonding and π "back-bonding". The latter results from the low-lying empty π* molecular orbital of CO interacting with a filled metal d orbital, helping the metal relieve itself of the electron density added during σ bond formation. Reducing the metal d-electron density by chemical oxidation or electronic excitation leads to a weakening of back-bonding, providing a means of triggering release of CO from the transition metal center. [6] Modifying the electronic properties of ancillary ligands through the introduction of electron-donating or electron-withdrawing groups also alters the M-CO bond strength, and thus the kinetics of CO release.[6, 10, 14]

Considerable research has been directed towards the development of light-activated CORMs (photoCORMs), which release CO only upon exposure to electromagnetic radiation.[9] A major benefit of this approach is that the intensity, shape, duration and direction of a light beam can be readily manipulated, enabling CO release to be controlled with extreme accuracy. Nowadays, the challenge lies in producing photoCORMs that can be activated with low energy wavelengths, i.e. preferably visible [15-17] or near-infrared light rather than UV radiation, since the latter is damaging to tissues and has low skin penetration depth. Different strategies to optimize the absorption profile of photoCORMs are under continued development and include extending the conjugation of

aromatic ligands, attachment of dyes, use of upconverting nanoparticles as energy transducers, or changing the metal ion.[18-19]

However, whilst major steps have been taken towards tailored prodrug design, relatively little information is available on the precise mechanism of CO release from photoCORMs.

Herein, we describe the results of an investigation into the UV-induced CO release characteristics of three ruthenium(II) carbonyl complexes, trans-(Cl) $[RuLCl_2(CO)_2]$ (L = 4,4'-dimethyl-2,2'-bipyridine (**1**), 4'-methyl-2,2'-bipyridine-4-carboxylic acid (**2**) or 4,4'-dicarboxylic acid-2,2'-bipyridine (**3**) (Figure 1). The ruthenium(II) bipyridine carbonyl motif is well known for its capacity to undergo photochemical decarbonylation,[20-24] and previous studies have shown that photolysis of such complexes in acetonitrile leads to successive formation of $[RuL(CO)(CH_3CN)Cl_2]$, $[RuL(CH_3CN)_2Cl_2]$, and $[RuL(CH_3CN)_3Cl]^+$ via photo-substitution processes.[20] Here, we wished to examine the influence of electron-donating/withdrawing methyl/carboxyl groups attached to the bipyridine ligand on the rates of photo-decarbonylation, as well as compare the rates of photolysis in organic (acetonitrile) and aqueous media (1% DMSO in H_2O). To this end, photolysis of each of the complexes was monitored by UV-Vis absorbance spectroscopy, with multivariate curve resolution-alternating least squares (MCR-ALS) analysis used to establish the number of reaction components and to extract quantitative kinetic information. Identification of the photochemical products has been aided by a combination of Fourier transform infrared (FTIR) spectroscopic measurements and density functional theory (DFT) calculations.

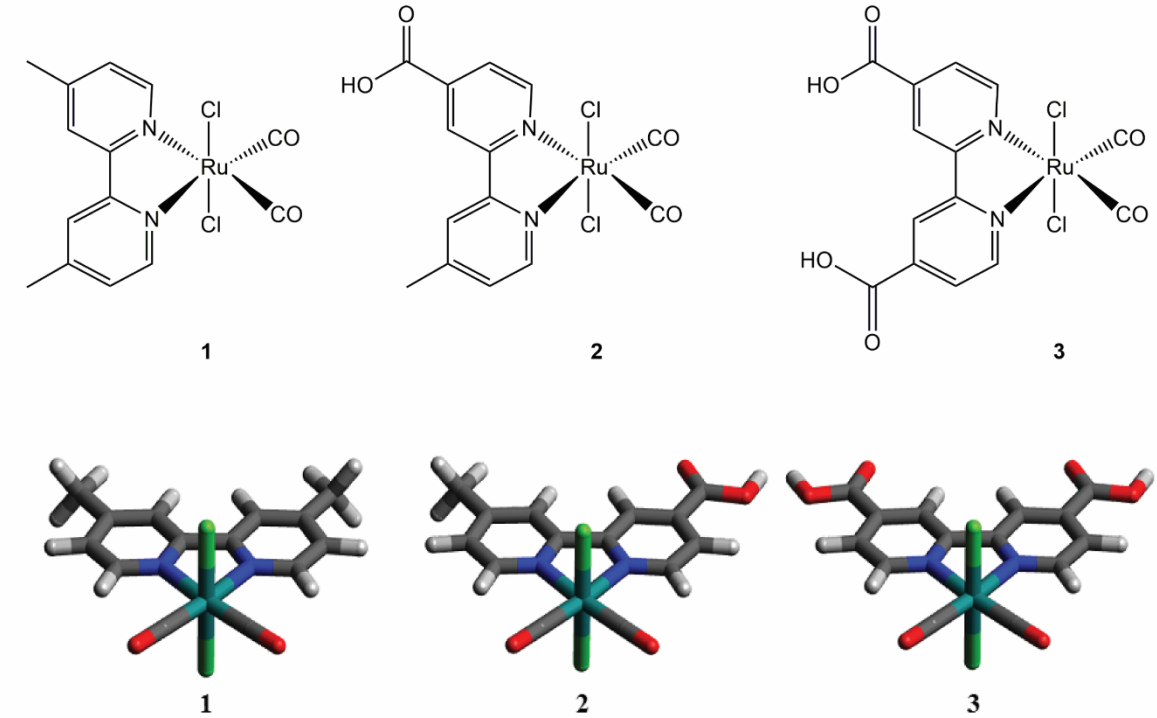

Figure 1. Chemical structures (top) and DFT energy-minimized structures (bottom) of the ruthenium(II) carbonyl complexes **1–3** investigated in this study.

EXPERIMENTAL DETAILS

Materials and reagents

Ruthenium trichloride hydrate was purchased from Strem Chemicals (cat. no. 44-5880). 4-Methyl-4’-carboxy-2,2’-bipyridine was purchased from Carbosynth Ltd. (cat. no. FM10294). 2,2’-Bipyridine-4,4’-dicarboxylic acid was purchased from Sigma-Aldrich (cat. no. 550566). Formic acid, 99% was obtained from Fluka. All solvents were purchased from reputable commercial suppliers (Sigma–Aldrich, Fluka, VWR, Fisher Scientific) and used without further purification. A Direct-Q 3 UV water purification system from Millipore (Merck KGaA) was used to produce ultrapure water. The resistivity of the ultrapure water was 18.2 MΩ·cm. HPLC-grade

or deuterated solvents were used for all spectral studies and degassed by purging with nitrogen for at least 30 min before use.

4,4'-Dimethyl-2,2'-bipyridine,[25-26] $[RuCl_2(CO)_2]_n$,[25] *trans*-(Cl) [Ru(4,4'-dimethyl-2,2'-bipyridine)$Cl_2(CO)_2$] (1),[25, 27] and *trans*-(Cl) [Ru(2,2'-bipyridine-4-carboxylic acid)$Cl_2(CO)_2$] (2)[28] were synthesized according to literature procedures. All characterization data were in agreement with that previously reported.

Physical Measurements

^1H and ^{13}C NMR spectra were measured at 298 K on Bruker DRX 400 spectrometers. Chemical shifts δ are reported in parts per million (ppm) relative to tetramethylsilane ($Si(CH_3)_4$). Coupling constants (*J*) are given in Hertz. Abbreviations for the peak multiplicities are as follows: s (singlet), d (doublet), dd (doublet of doublets), t (triplet), and m (multiplet). UV-Vis absorbance spectra were recorded on a Cary 300 spectrophotometer (Agilent Technologies) using a 1 nm step-size. ESI-MS was carried out on Agilent 6120 Series Quadrupole LC/MS system.

FTIR Spectroscopy

Attenuated total reflectance (ATR)-FTIR spectra were acquired on a Bruker model Equinox 55 FT-IR spectrometer fitted with a N_2-cooled mercury-cadmium-telluride (MCT) detector. A Harrick silicon multiple reflection ATR (Si-ATR) accessory was used for spectral acquisition. The silicon ATR accessory is transparent in the CO vibrational region. Aliquots (10 μL) of acetonitrile solutions of the complexes (1 mg mL^{-1}) were deposited on the silicon ATR, followed by evaporation (5 min) under a gentle N_2 flow, resulting in a thin film of compound for direct measurement. The spectra were acquired with OPUS software 6.0. ATR spectra were collected in the wavenumber range between 4000–600 cm^{-1} at a spectral resolution of 4 cm^{-1} and 50 interferograms were co-added.

Data Processing

Pre-processing of the spectral data was performed in OPUS software 7.2. ATR-FTIR spectra were baseline corrected using concave rubberband correction.

Multivariate Curve Fitting Analysis

UV-Vis absorbance spectra for all time points were imported into a Matlab matrix. The Matlab Toolbox MCR-ALS 2.0[29] was used to estimate the number of components by the inbuilt singular value decomposition (SVD) algorithm and to extract the spectrum and transient concentration development of each component using a multivariate curve resolution-alternating least squares (MCR-ALS) algorithm.[30] The number of components was determined from the number of Eigenvalues ≥ 1, and confirmed later by manual variation of the number of components, available time points and an adapted kinetic model constraint. The initial estimates of the spectra were determined by means of the purest variable detection method. The following constraints were set for the ALS optimization: (i) non-negativity for all species concentration and spectra via non-negative least square (nnls), and (ii) a kinetic constraint to correlate the different species via a consecutive kinetic model, $A \rightarrow P_1 \ldots \rightarrow P_i$ with k_i (Scheme 2), with the pre-defined number of species. At the beginning, only one species exists and therefore only the initial concentration (of species A) was different from zero and set to 60 µM. Estimates for the reaction rate constant were $k_1 = 2.7\ min^{-1}$, $k_2 = 0.17\ min^{-1}$ and $k_3 = 0.05\ min^{-1}$. No normalization was applied and convergence was typically achieved in less than 100 iterations with a convergence limit of $10\ e^{-3}$.

Theoretical Calculations

DFT calculations were performed using the GAUSSIAN09 package[31] with the hybrid Perdew–Burke–Ernzerhof exchange correlation functional with 25% HF (PBE0). A mixed basis set is used where a cc-pVDZ basis set was used for carbon, hydrogen, nitrogen, oxygen and chloride and an

augmented cc-pVDZ-PP basis set[32] with effective core potentials (ECP) including two f polarization functions for ruthenium. Geometry optimization of the ground-state (S_0) of complexes **1**–**3** were performed using the conductor-like polarizable continuum model (CPCM) with acetonitrile as the solvent.[33-35] By allowing all parameters to relax, the calculations converged to optimized geometries corresponding to true energy minima, as revealed by the lack of imaginary values in the vibrational mode calculations. A full conformation screening was performed on complexes **1**–**3** and acetonitrile derivatives of **2** without any symmetry restrictions for the respective complexes until corresponding minima were attained. Ground-state lowest energy geometries computed by theoretical calculations using CPCM were compared to the previously reported crystal structures.[36-37] Low-lying excited states were calculated using time-dependent DFT (TD-DFT) on the optimized S_0 geometries. The first fifty vertical singlet excited states of the optimized S_0 geometries were calculated using TD-DFT. UV-Vis absorbance spectra, and molecular orbitals, and calculated FTIR wavenumber values and intensities were exported from GaussView 5.[38]

Photolysis Experiments

The photolysis experiments were conducted using a Rayonet Photoreactor (RPR-200 model) fitted with two Rayonet lamps with an emission wavelength centered at 350 nm (FWHM = 45 nm, $E_v \approx 2.5$ mW $\cdot$ cm^{-2}). A 1-cm quartz fluorescence cuvette (3 mL) was used as the reaction vessel. The power density was measured using a power meter with a built-in photodiode sensor (PM200 Series) from Thorlabs. The rate of CO release upon exposure of UV light was measured by recording the UV-Visible absorption spectra (250–800 nm) of complexes **1**–**3** in acetonitrile or 1% (*v*/*v*) DMSO in H_2O for certain time intervals. All experiments were performed in duplicate or triplicate.

Syntheses

All reactions were performed under nitrogen atmosphere using standard Schlenk techniques and assemblies were protected from light if necessary by wrapping them with aluminium foil.

trans-(Cl) [Ru(2,2'-bipyridine-4,4'-carboxylic acid)$Cl_2(CO)_2$] (**3**). A suspension of 2,2'-bipyridine-4,4'-carboxylic acid (50 mg, 0.21 mmol) in DMF (5 mL) was refluxed for 20 min and then $[RuCl_2(CO)_2]_n$ (46 mg) in DMF (2 mL) was added. After adding the polymer, the suspension was refluxed for another 20 min and then stirred at r.t. over the weekend under a nitrogen atmosphere and with the exclusion of light. The orange-brown solution was filtered and evaporated *in vacuo*. The residue was dissolved in a minimum amount of methanol (3 mL) and stored in the fridge to allow precipitation. The precipitate was filtered and dried under high vacuum to yield 3 (23 mg, 23%) as an orange solid. ^{1}H NMR (400 MHz, acetone-d_6): δ 9.40 (d, 2H, ^3J = 5.6 Hz), 9.13 (s, 2H), 8.37 (dd, 2H, ^3J = 5.6 Hz, ^4J = 1.6 Hz) ppm. MS (ESI$^-$): *m/z* 472.9 [M-H]$^-$. FTIR (Si-ATR): 2069 (s, C≡O), 2002 (s, C≡O) 1741 (s, C=O) cm^{-1}. These results are in agreement with the reported ones.[22]

RESULTS AND DISCUSSION

The bipyridine ligands bearing methyl and/or carboxylic acid groups were synthesized according to the literature[25-26] or were purchased from commercial suppliers. The ruthenium(II) carbonyl complexes (Figure 1) were prepared by reacting the key polymeric precursor $[RuCl_2(CO)_2]_n$ (prepared from $RuCl_3.xH_2O$ and paraformaldehyde)[25] with the respective bipyridine ligand, under an inert atmosphere and excluding light, following well-established protocols (Scheme 1).[21, 24-25, 39-41] In the case of complexes **1** and **2**, methanol was used as the solvent. Highest yields (30–40%) were obtained when the $[RuCl_2(CO)_2]_n$ was refluxed in the methanol prior to addition of the bipyridine ligand.[42] This procedure avoids the formation of a ruthenium(II) methoxycarbonyl

species, which is formed as a byproduct from the tricarbonyl species $[RuCl_2(CO)_3]_2$ existing as an impurity in the ruthenium polymer.[41-43] In the case of **3**, DMF was used as the solvent due to limited solubility of 2,2'-dicarboxylic acid-4,4'-bipyridine in methanol; a yield of 23% was obtained. ESI-MS and ^{1}H NMR spectroscopy confirmed the formation of the complexes. In each case, coordination of the ligand to the diamagnetic ruthenium(II) center produced a slight upfield shift in the positions of the aromatic signals in the ^{1}H NMR spectrum (Figures S1–3). The lowest energy ground-state geometries of the complexes were computed by DFT calculations (Figure 1), as described in the Experimental Section (see Tables S1–3 for Cartesian coordinates). Selected bond distances and angles are reported in Table S4, together with the corresponding values observed in previously reported crystal structures.[36-37] In general, the calculated geometries are in good agreement with the experimental data.

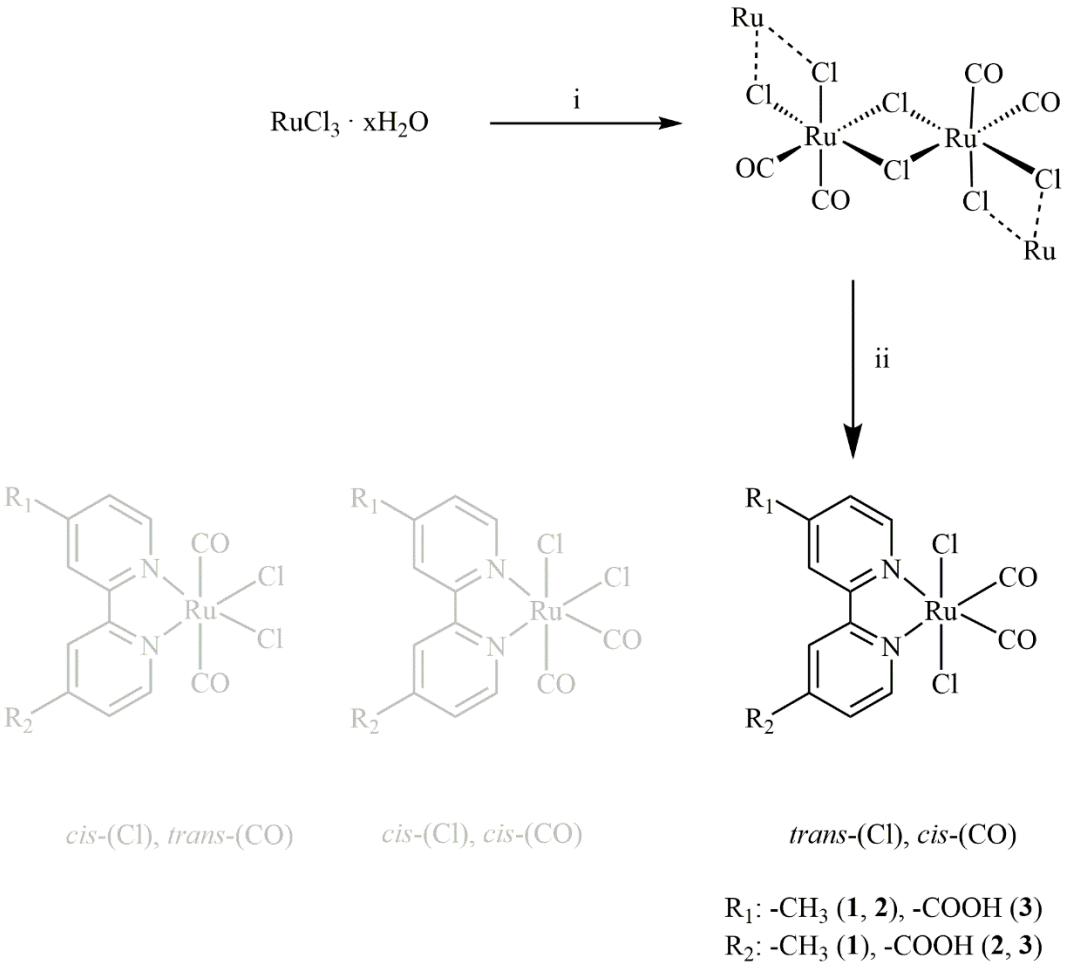

Scheme 1. Synthesis of complexes **1–3** (in grey: possible isomers not formed by this procedure). Reagents and conditions: i) paraformaldehyde, 99% formic acid, reflux, o/n, 70%; ii) respective bipyridine ligand, methanol for **1** and **2**, DMF for **3**, reflux, 1 h, 23–40%.

Electronic absorption spectra of complexes

The UV-Vis absorption spectra of complexes **1**–**3** were recorded in acetonitrile and 1% (*v*/*v*) DMSO in H_2O and are shown in Figure **2** and Figure **3**, respectively. All of the complexes show three main absorption bands in acetonitrile, with two bands below 350 nm and one above. By anchoring electron-withdrawing groups to the bipyridine scaffold, bathochromic shifts in all absorption maxima were observed, e.g., λ_{max} = 349 nm for 1 in comparison to λ_{max} = 362 nm for

2 and λ_{max} = 378 nm for 3. The extinction coefficients for all transitions, as well as at a wavelength of 350 nm, are reported in Table 1.

Table 1. Absorption maxima and molar extinction coefficients for complexes **1–3** in acetonitrile and 1% (*v*/*v*) DMSO in H_2O

Solvent	**Complex**	**$\varepsilon\,\lambda_{max}$ [M^{-1} cm^{-1}] (λ_{max} [nm])**	**$\varepsilon\,\lambda_{max}$ [M^{-1} cm^{-1}] (λ_{max} [nm])**	**$\varepsilon\,\lambda_{max}$ [M^{-1} cm^{-1}] (λ_{max} [nm])**	**$\varepsilon_{350\ nm}$ [M^{-1} cm^{-1}]**
Acetonitrile	**1**	8500 ± 200 (298)	10500 ± 190 (310)	1300 ± 90 (349)	1300 ± 100
	2	9500 ± 100 (310)	8800 ± 100 (322)	1900 ± 50 (362)	1800 ± 80
	3	10900 ± 640 (316)	10700 ± 760 (329)	2200 ± 140 (378)	1800 ± 100
1% (*v*/*v*) DMSO	**1**	10600 ± 320 (299)	13300 ± 290 (311)	-	1100 ± 200
	2	-	12300 ± 350 (319)	-	900 ± 120
	3	12600 ± 220 (314)	13400 ± 170 (325)	-	1400 ± 270

The UV-Vis spectra of **1**–**3** in 1% (*v*/*v*) aq. DMSO show only two bands in the UV region and one shoulder around 350 nm, which is also shifted to a higher wavelength when more electron-withdrawing groups are attached to the bipyridine ligand (Figure 3). The absorption maxima and extinction coefficients (Table 1) are similar to those determined in acetonitrile.

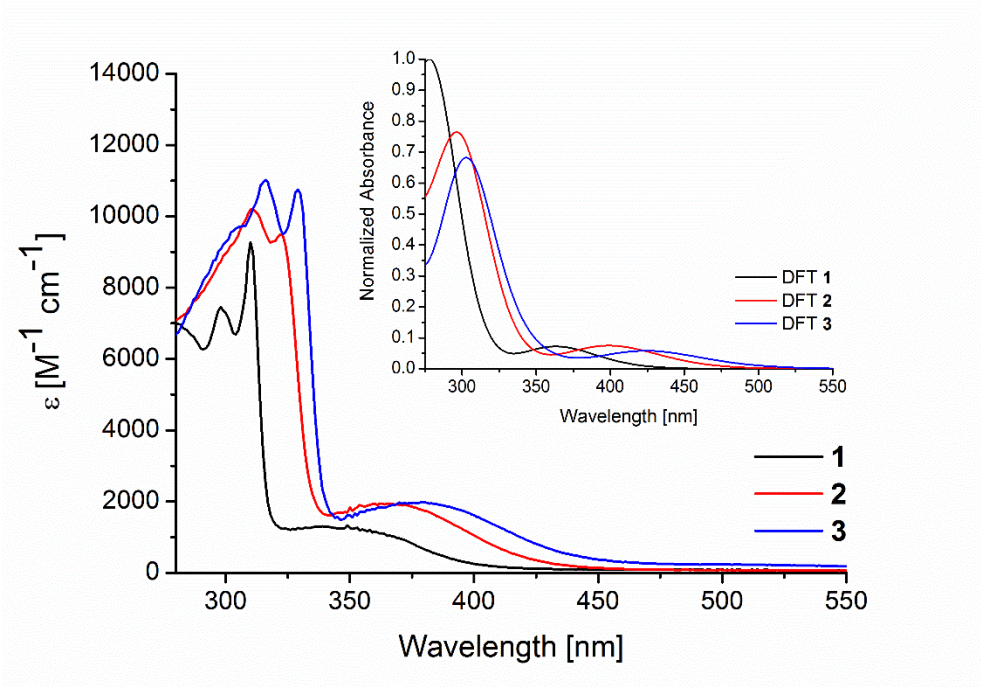

Figure 2. UV-Vis absorption spectra measured for **1** (66 µM), **2** (57 µM) and **3** (47 µM) in acetonitrile, and predicted from TD-DFT calculations (inlet).

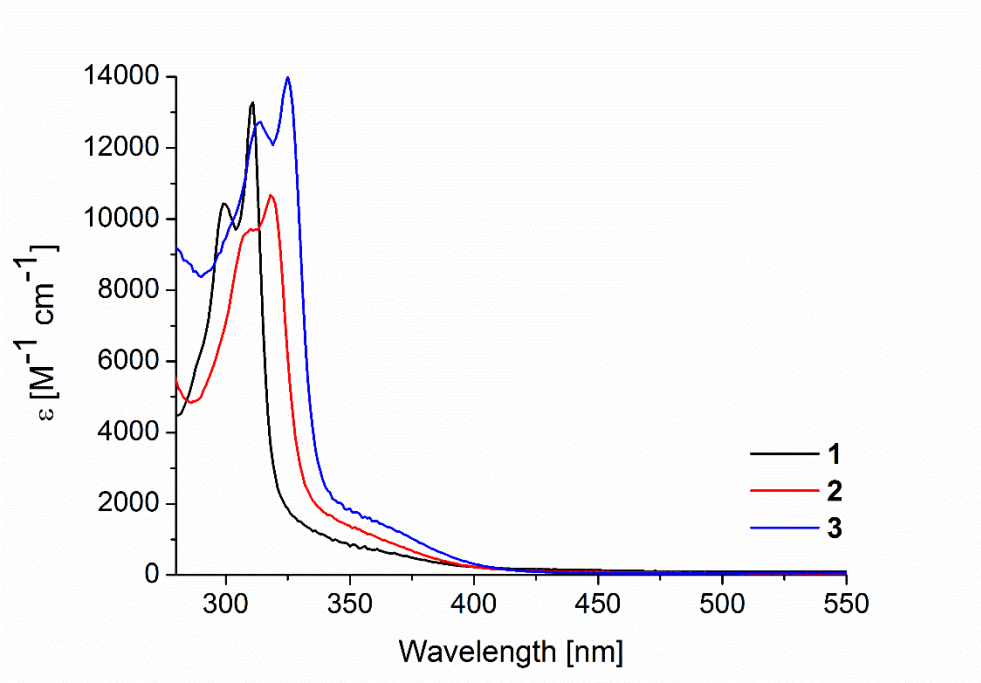

Figure 3. UV-Vis absorption spectra measured for **1** (58 µM), **2** (62 µM) and **3** (53 µM) in 1% (*v*/*v*) DMSO in water.

Also shown in Figure 2 (inlet) are the absorption spectra predicted from time-dependent DFT (TD-DFT) calculations. These reproduce the observed spectra well, with the calculated absorption maxima within the accepted margin of error for such TD-DFT calculations of ca. 0.3 eV.[44] In general, the bathochromic shifts observed in moving from complex **1** to **3** were well captured by the calculations.

The transitions predicted by the TD-DFT calculations are reported in Table S5. The lowest energy transition (exp: 349 nm, 362 nm, 378 nm, calcd: 364 nm, 399 nm, 423 nm for **1**, **2** and **3**, respectively) is a mixed (Ru, Cl-to-π*bpy) metal-to-ligand and ligand-to-ligand charge transfer (MLCT/LLCT) band, which originates from an almost pure HOMO-1 (highest occupied molecular orbital)-to-LUMO (lowest unoccupied molecular orbital) excitation (Figure 4 and Figure S4; note that the calculated molecular orbitals for **1**, **2** and **3** are highly similar and therefore only the molecular orbitals of **2** are shown in Figure S4). The other two experimentally observed electronic transitions (310/298 nm, 322/310 nm and 329/316 nm for **1**, **2** and **3**, respectively) can be attributed to the strong πbpy-to-π*bpy LLCT bands predicted at 288/278 nm, 297 nm and 303 nm, respectively. Interestingly, two strong bands are predicted for complex **1**, centered at 288 nm and 279 nm (Table S2), which are mixed LLCT/MLCT bands (HOMO-2-to-LUMO, πbpy-to-π*bpy and HOMO-to-LUMO+1, Ru, Cl-to-π*bpy). In contrast, for complexes **2** and **3**, the predicted transitions at 297 nm and 303 nm, respectively, are nearly pure LLCT bands (HOMO-2-to-LUMO, πbpy-to-π*bpy). The MLCT bands corresponding to the HOMO-to-LUMO+1, Ru, Cl-to-π*bpy transition are predicted to be of weak intensity and centered at 320 nm and 337 nm, respectively. The energy difference between HOMO-1 and LUMO decreases with the introduction of the

electron-withdrawing carboxyl groups onto the bipyridine ligand, which is in accord with the observed red-shift in the Ru, Cl-to-π*bpy MLCT/LLCT band.

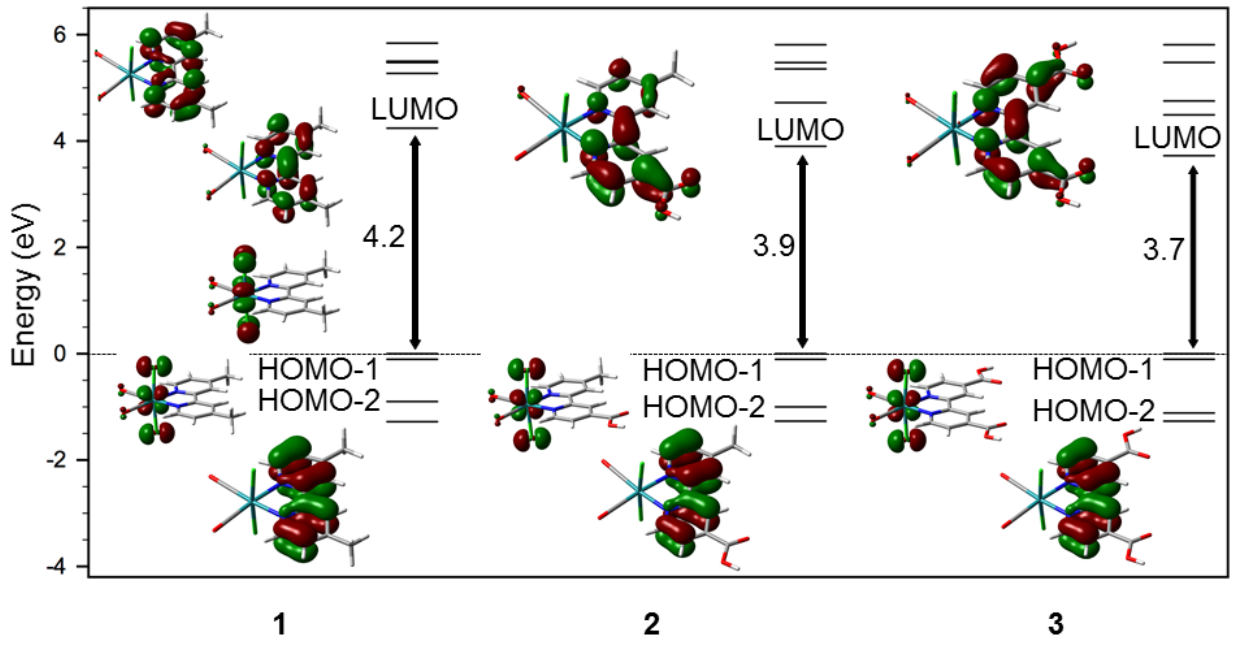

Figure 4. DFT-derived molecular orbital diagrams for complexes **1**–**3**. The orbitals are arranged with respect to the HOMO at 0 eV (HOMO-3 to LUMO+4).

Photo-induced CO release monitored by electronic absorption spectroscopy

The UV light-induced CO release characteristics of the complexes were studied in the two different solvent systems (acetonitrile and 1% (v/v) DMSO in H_2O) by following the changes in the UV-Visible absorption spectra upon exposure to 350 nm radiation. Prior to this, measurements performed on samples stored in the dark and under air revealed no spectral changes over a period of two months, indicating that the complexes are highly stable in aerated solution in the absence of light. Upon even brief exposure to UV light ($E_v \approx 2.5$ mW $\cdot$ cm^{-2}) (< 1 second), however, significant colour changes were observed (yellow to orange-red). Due to the limitations of the

experimental set-up, we were not able to record spectra within less than 10 s of irradiation. Typically the first absorbance measurement was performed after 30 s of irradiation.

The absorption spectra of the irradiated solutions of complexes **1**–**3** in acetonitrile are shown in Figure 5. Three bands of increasing intensity were observed within the first 10 min, 30 min and 3 min of irradiation for **1**, **2** and **3**, respectively (Figure 5, left). The band with a λ_{max} of 350–375 nm is referred to as **b1**, and the one with a λ_{max} of 500–600 nm as **b2**. After these times, bands **b1** and **b2** reduced in intensity and a new band, **b3**, with a λ_{max} between 425–450 nm appeared (Figure 5, right). A red-shift in the λ_{max} values for each of the bands was observed in moving from complex **1** to **2** to **3**. Three isosbestic points were observed for **1** and **2**, whereas only one occurred for **3**. No more significant changes in the spectra occurred after 40 min, 4 h and 2 h for **1**, **2** and **3**, respectively.

Table 2. Fitted rate constants and half-lives for photolysis of complexes **1**-**3** in acetonitrile and in 1% (*v*/*v*) DMSO in H_2O exposed to 350 nm radiation ($E_v \approx 2.5$ mW · cm^{-2}) at r.t.

	Complex in acetonitrile			**Complex in 1% (*v*/*v*) DMSO**		
	1	**2**	**3**	**1**	**2**	**3**
k_1 **[min^{-1}]**	2.9 ± 0.2	5.1 ± 0.2	3.3 ± 0.4	0.46 ± 0.05	1.3 ± 0.1	2.0 ± 0.1
τ (min)	(~0.24)	(~0.14)	(~0.21)	(~1.5)	(~0.5)	(~0.35)
k_2 **[min^{-1}]**	0.17 ± 0.02	0.11 ± 0.01	0.099 ± 0.007	0.026 ± 0.003	0.035± 0.007	0.027 ± 0.005
τ (min)	(~4)	(~6)	(~7)	(~27)	(~20)	(~26)
k_3 **[min^{-1}]**	0.048 ± 0.002	0.006 ± 0.001	0.001 ± 0.001	-	-	-
τ (min)	(~14)	(~116)	(~693)			

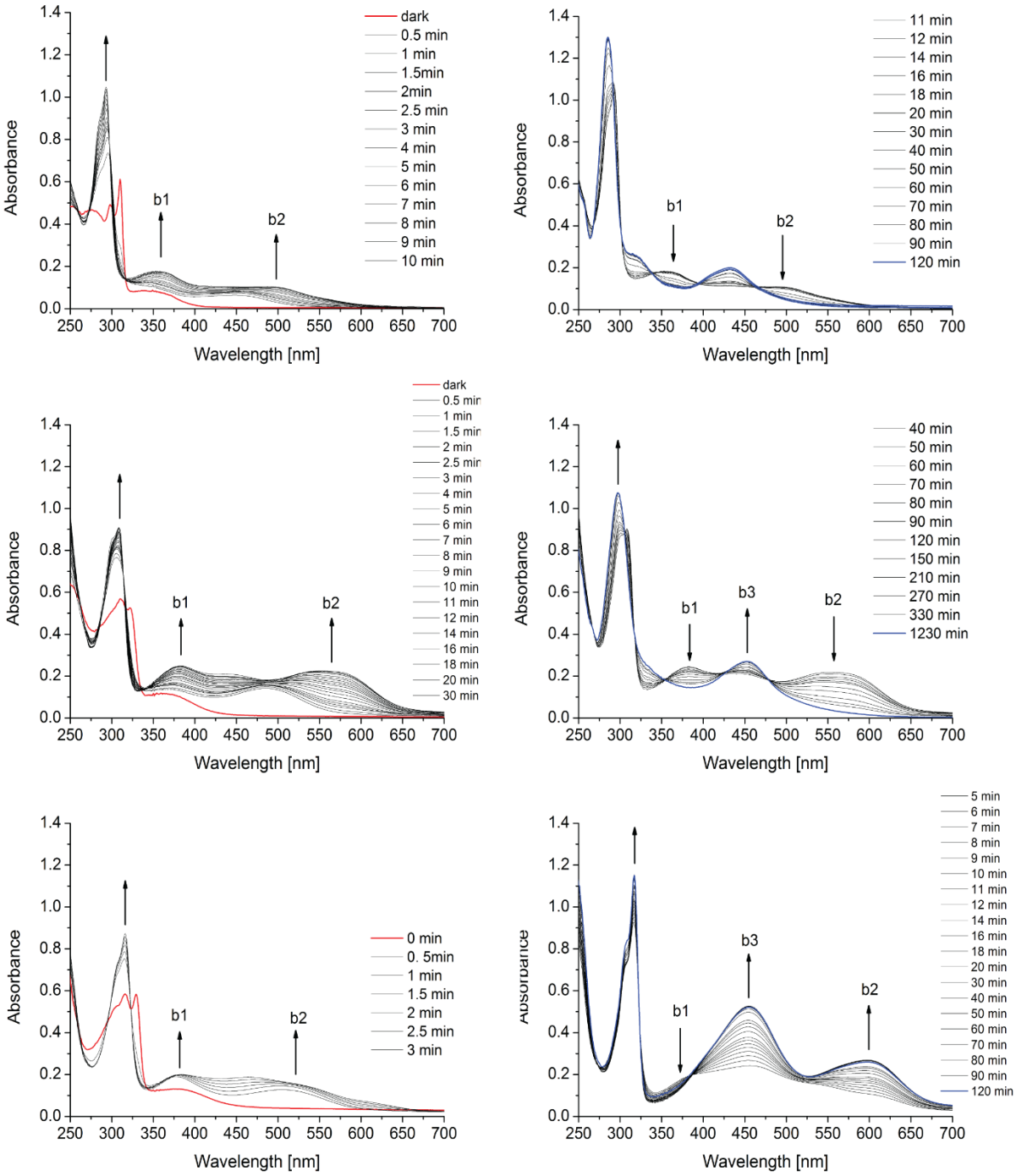

Figure 5. UV-Vis absorption spectra measured for **1** (66 µM; top), **2** (57 µM; middle) and **3** (69 µM; bottom) in acetonitrile after different periods of exposure to 350 nm radiation ($E_v \approx 2.5$ mW · cm^{-2}) at r.t.

To elucidate the mechanism and kinetics of photolysis, the UV-Vis absorption spectra were analysed by MCR-ALS analysis, as described in the Experimental Section. A kinetic model with three consecutive steps and four individual compounds was able to account for the observed changes in the spectra (Scheme 2), with the fitted spectra being hardly distinguishable from the experimental spectra at each given time point because numerical fitting errors were smaller than 2% (see Figures S5–10). The fitted spectra and concentration profiles for complexes **1**–**3** and their photoproducts are shown in Figure 6.

Our results are consistent with those of a previous study, which showed that the photolysis of *trans*-(Cl) [Ru(bpy)$Cl_2(CO)_2$] (A) in acetonitrile leads to successive formation of [Ru(bpy)(CO)(CH_3CN)Cl_2] (P_1), [Ru(bpy)(CH_3CN)$_2Cl_2$] (P_2), and [Ru(bpy)(CH_3CN)$_3$Cl]$^+$ (P_3).[20] In support of this mechanism, we found that the UV-Vis absorption spectra predicted for these complexes by TD-DFT calculations were consistent with the MCR-ALS-extracted spectra for species A, P_1, P_2 and P_3 (Figure S11).

$$A \xrightarrow{k_1} P_1 \xrightarrow{k_2} P_2 \xrightarrow{k_3} P_3$$

Scheme 2. Serial mechanism for the photoreaction of complexes **1**–**3** (A: starting complex; P_1, P_2, P_3: photo-products).

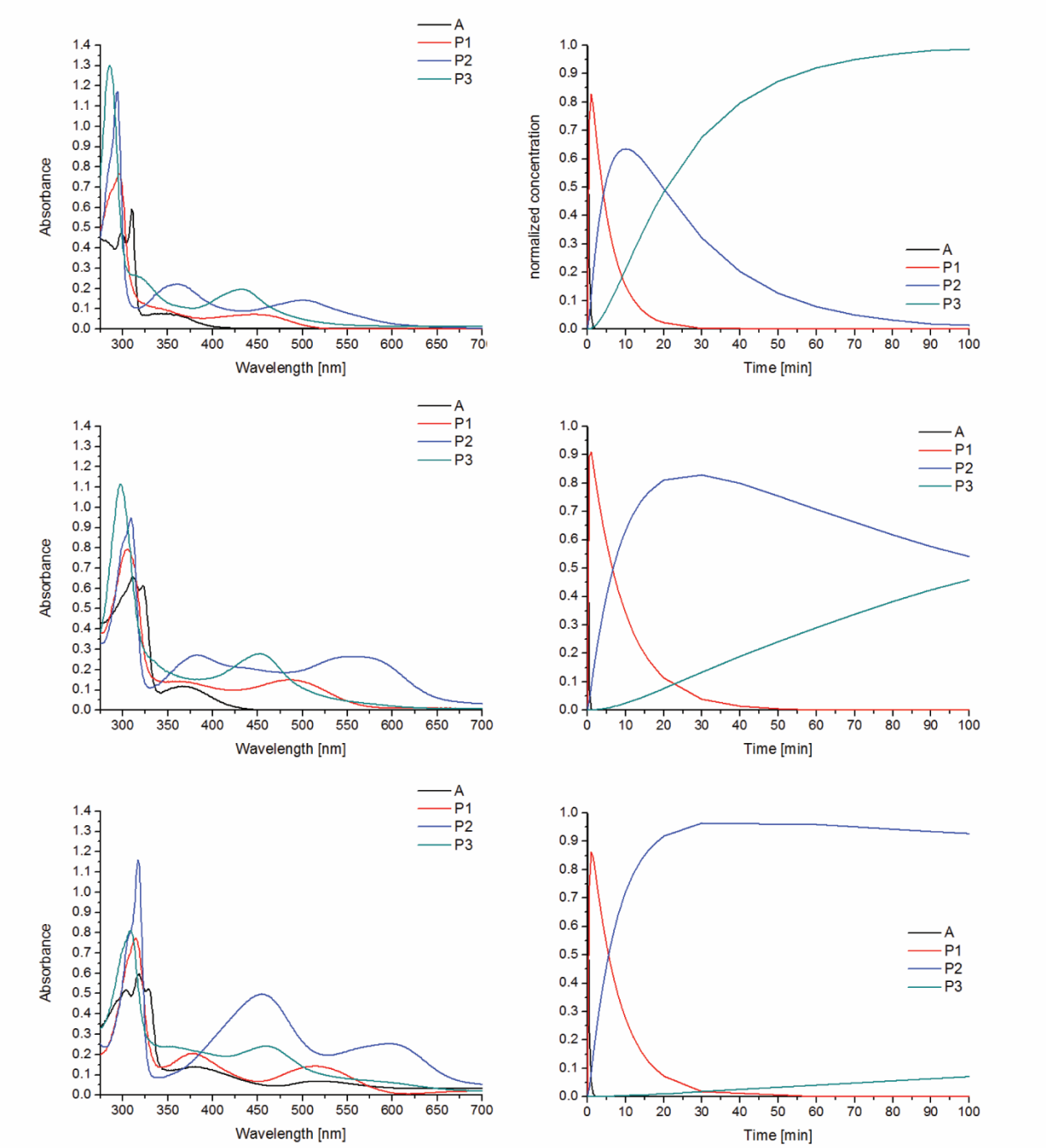

Figure 6. UV-Visible absorption spectra and concentration profiles for complexes **1**–**3** (A) and the associated photoproducts (P_1, P_2, P_3), derived by fitting the experimental data to the model presented in Scheme 2 using MCR-ALS analysis (top: complex **1**, middle: complex **2**, bottom: complex **3**.

The reaction rate constants and species half-lives associated with the photolysis of complexes **1**–**3** are collated in Table 2. The first reaction occurs very quickly, i.e., the absorption spectra change drastically upon initial irradiation. Thus, often only two spectra were available for the fit and consequently the rate constants are considered to be a lower limit only (k_1 >> 3 min^{-1}). In fact, a picosecond time-resolved infrared spectroscopic and DFT computational study has previously established that the transformation of *trans*-(Cl) [Ru(bpy)$Cl_2(CO)_2$] into the initial photoproduct, [Ru(bpy)(CO)(CH_3CN)Cl_2], occurs within the order of picoseconds, via a pentacoordinate intermediate, *trans*(Cl)-[Ru(bpy)(CO)Cl_2].[21] The second rate constant k_2 is much smaller in magnitude and decreases from 0.17 min^{-1} to 0.11 min^{-1} and then 0.099 min^{-1} for the series **1**–**3**, indicating that the electron-withdrawing carboxyl groups slow the release of the second CO molecule to generate [RuL(CH_3CN)$_2Cl_2$] (P_2) from [RuL(CO)(CH_3CN)Cl_2] (P_1). The third rate constant k_3, corresponding to the substitution of a chloro ligand by a solvent molecule to generate [RuL(CH_3CN)$_3$Cl]$^+$ (P_3), is smaller again still, and follows the trend k_3 (**1**) > k_3 (**2**) > k_3 (**3**).

Photolysis of complexes **1**–**3** was also performed in a water/DMSO mixture to mimic biological conditions (Figure 7).

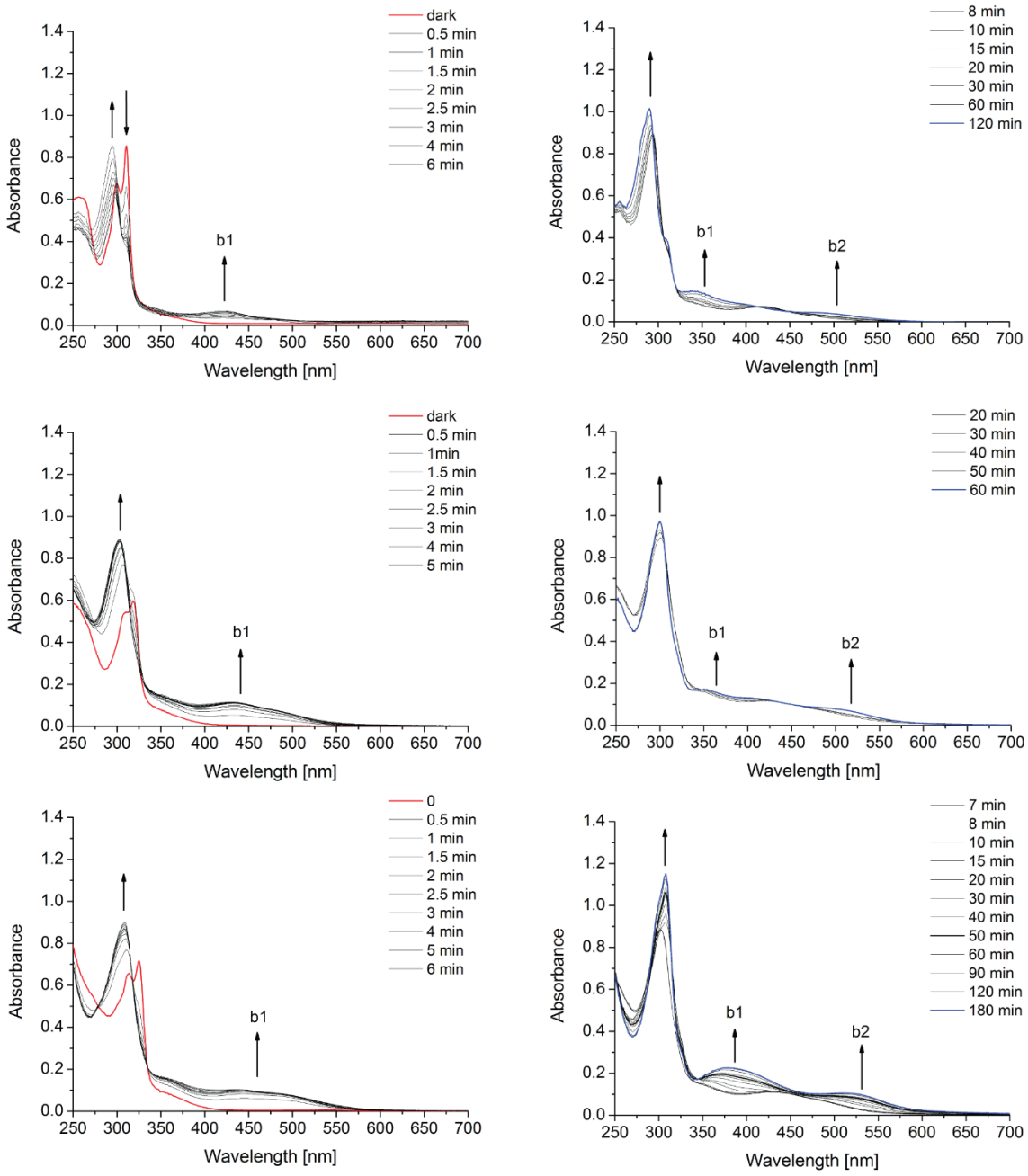

Figure 7. UV-Vis absorption spectra measured for **1** (64 µM; top), **2** (47 µM; middle) and **3** (54 µM; bottom) in 1% (*v*/*v*) DMSO in H_2O after different periods of exposure to 350 nm radiation ($E_v \approx 2.5$ mW · cm^{-2}) at r.t.

The complexes all showed less changes in absorption profile compared to the photolysis experiments in acetonitrile. During the first minutes of irradiation (0.5–10 min), one of the UV bands increased in intensity and underwent a slight hypochromic shift (~15 nm), whereas the second UV band (**1** and **3**) or shoulder (observed for **2**) decreased in intensity. Meanwhile, a new band, **b1**, formed in the visible region between 400–500 nm (Figure 7, left). A red-shift in the λ_{max} value for this band was observed in moving from complex **1** to **2** to **3**. After a certain time, this band disappeared and two new bands, **b2** and **b3**, appeared in the visible region (Figure 7, right). These two bands are centred at ~350 nm and ~525 nm for each of the complexes, but are less distinct for the irradiated species **1** and **2**. Using MCR-ALS analysis, the data could be fitted to a two-step reaction model, yielding the rate constants presented in Table 2. The fitted spectra and concentration profiles are shown in Figure 8. It is proposed that these two steps correspond to the formation of $[RuL(CO)(H_2O)Cl_2]$ and $[RuL(H_2O)_2Cl_2]$, given that the spectral changes are broadly similar to those observed in the first two steps of the photolysis reaction in acetonitrile (Figure 5, left). In each case, the first rate constant k_1 is again much larger than the second one, indicating that the release of the first CO molecule occurs much more readily than the second. Clearly, the decarbonylation steps are significantly slower in aqueous medium compared to acetonitrile. The influence of the carboxyl groups (complexes **2** and **3**) on the rate of these reactions is also less clear-cut in aqueous medium.

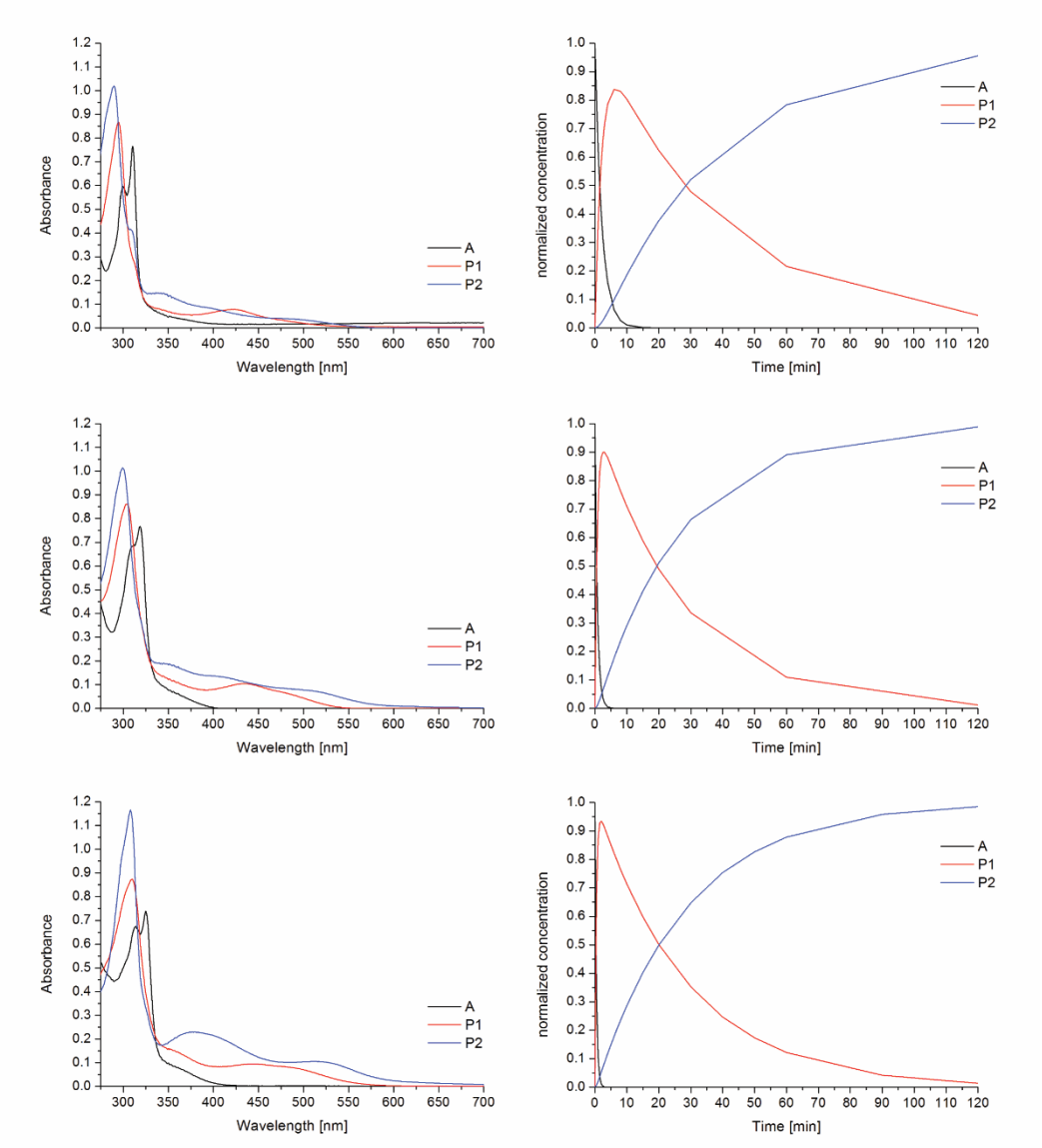

Figure 8. UV-Visible absorption spectra and concentration profiles for complexes **1**–**3** (A) and the associated photoproducts (P_1, P_2), derived by fitting the experimental data to a two-step model using MCR-ALS analysis (top: complex **1**, middle: complex **2**, bottom: complex **3**).

Fourier transform infrared spectra of complexes

The FTIR spectra of complexes **1**–**3** (Figure S12) show two strong CO vibrations in the expected region (2100–1900 cm-1), with the higher energy band assigned to the symmetric stretching mode, and the lower to the anti-symmetric one (Table 3). These bands are shifted to a slightly higher

frequency for complexes **2** and **3** due to the inductive electron-withdrawing effects of the carboxyl groups present within the bipyridine ligands.

Table 3. CO vibrations observed in the FTIR spectra of complexes **1**–**3**.

Complex	**ν_{sym}(CO) [cm^{-1}]**		**ν_{asym}(CO) [cm^{-1}]**	
	Exp[1]	**Calcd[2]**	**Exp[1]**	**Calcd[2]**
1	2054	2059	1985	1993
2	2065	2062	1999	1999
3	2069	2065	2002	2002

[1] Measured via Si-ATR-FTIR spectroscopy. [2] Calculated from DFT calculations, with a uniform scaling factor of 0.965 applied.

Table 3 also shows the anti-symmetric and symmetric ν(CO) values predicted from TD-DFT calculations. Excellent agreement between the experimental and calculated values was found after a uniform scaling factor of 0.965 was applied to the raw computed values to address the absence of anharmonicity in the theoretical description.[45-46]

Photo-induced CO release monitored by Fourier transform infrared spectroscopy

The UV light-induced CO release characteristics of the complexes in acetonitrile were also assessed by FTIR spectroscopy. FTIR spectra of the irradiated complexes were recorded after depositing an aliquot of an irradiated complex solution onto a silicon attenuated total reflectance (ATR) accessory and drying with N_2 gas. The changes observed in the characteristic CO region (2150–1900 cm^{-1}) of the infrared spectrum upon irradiation of the complexes are shown in Figure 9 (see Table S6 for frequency values).

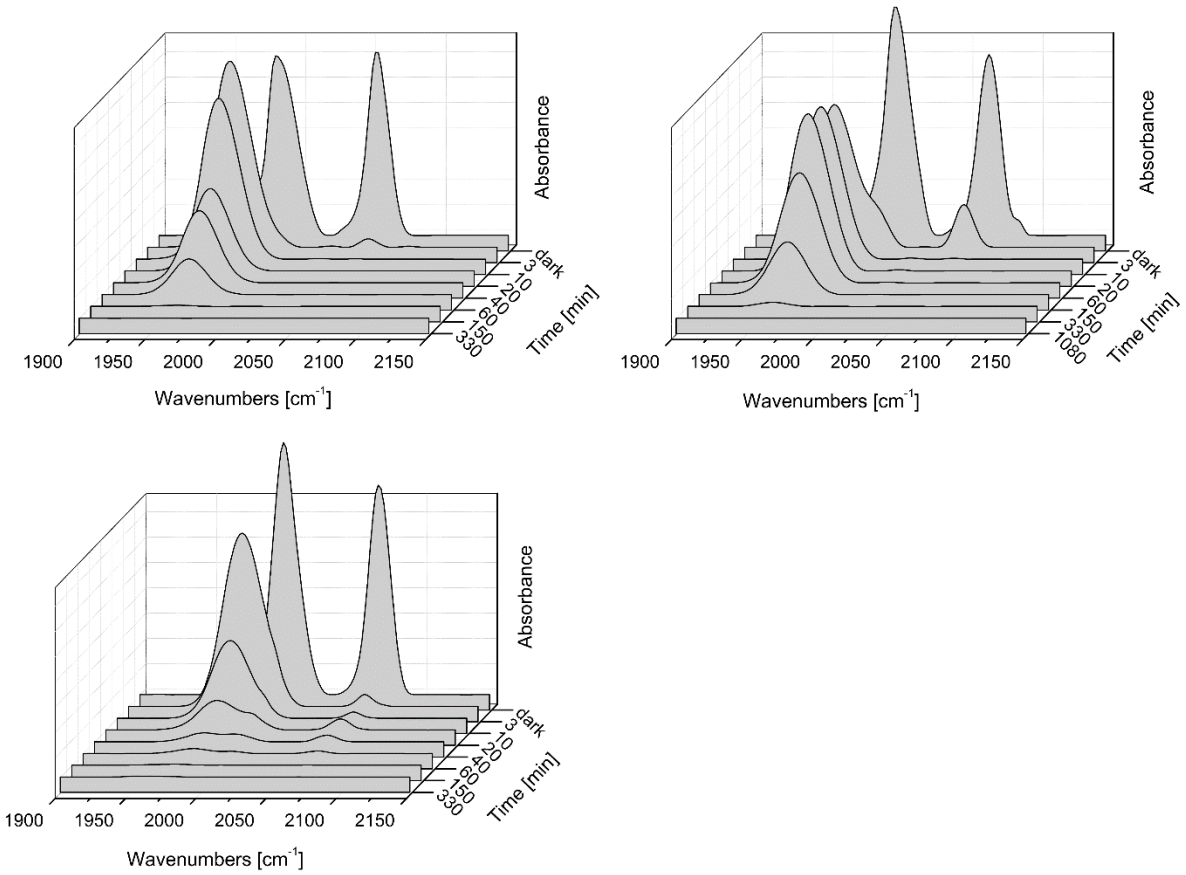

Figure 9. FTIR spectra (2150–1900 cm^{-1}) measured for **1** (top left), **2** (top right) and **3** (bottom left) after different periods of exposure to 350 nm radiation in acetonitrile.

For each complex, the rapid color change from yellow to orange-red observed upon exposure to UV light was seen to be accompanied by a dramatic decrease in the intensities of the two CO bands associated the starting complex, together with the appearance of an intense new band at 1963 cm^{-1} for **1** and **2**, and at 1981 cm^{-1} for **3**. DFT calculations support the hypothesis that these spectral changes are associated with the release of the first CO molecule from the staring complex to generate $[RuL(CO)(CH_3CN)Cl_2]$ (P_1) – the CO stretching vibration for a structure containing one CO and one acetonitrile ligand is predicted to occur at 1971–1980 cm^{-1} (Figure S13). The coordinated acetonitrile ligand was evident from a band at 2270–2280 cm^{-1} (Table S3),

compared to *ca.* 2252 cm^{-1} for non-coordinating acetonitrile. The intensity of the CO band associated with the monocarbonyl species progressively diminished with time, indicating release of the second CO molecule within the time course of the experiments. After 2.5–5.5 h of irradiation, decarbonylation of the complexes was complete. Taken together, the FTIR data are consistent with the photolysis mechanism discussed above.

CONCLUSION

A fundamental understanding of the mechanism of CO release from photoCORMs is essential for their exploitation as therapeutics. Here we have shown that data obtainable from spectroscopic techniques such as electronic absorption spectroscopy and FTIR spectroscopy can be analyzed with chemometric tools like MCR-ALS to extract kinetic and mechanistic information and thereby improve our understanding of the structural aspects influencing photoreactivity.

We found that the UV-triggered release of a first CO molecule from *trans*-(Cl) $[RuLCl_2(CO)_2]$ complexes in acetonitrile occurs very rapidly, to the extent that we could not determine the influence of electron-donating/withdrawing groups attached to the bipyridine ligand on the rate of reaction with our current experimental set-up. The release of the second CO molecule was considerably slower, and electron-withdrawing carboxyl groups were found to reduce the rate of decarbonylation. The introduction of such groups increased the absorbance maxima, which may have the advantage of enabling more “biologically friendly” longer wavelength light to be used for excitation. The rate of decarbonylation was also found to be significantly slower in aqueous media, highlighting once again that results obtained using organic solvents may not be directly translatable to the biological/medicinal realm.

ASSOCIATED CONTENT

Supporting Information

^{1}H NMR spectra of complexes **1**–**3** in deuterated acetone; Cartesian coordinates for DFT-calculated ground-state geometries of complexes **1**–**3**; selected bond distances (Å) and angles (°) for the DFT-calculated structures of complexes **1**–**3** and two reported crystal structures[36-37]; selected low-lying electronic transitions of complexes **1**–**3** predicted by TD-DFT calculations; main molecular orbitals of complex **2** involved in the electronic transitions; comparison of MCR-ALS fit and experimental UV-Vis absorbance spectra recorded upon UV irradiation of complexes **1**–**3** in acetonitrile and 1% DMSO in water; comparison of MCR-ALS-derived and TD-DFT-predicted UV-Vis absorbance spectra for proposed photoproducts of **2** in acetonitrile; infrared spectra of complexes **1**–**3**; selected infrared bands observed upon UV irradiation of complexes **1**–**3** in acetonitrile; and simplified representation of complex **2** and its acetonitrile-substituted derivatives, together with the corresponding carbonyl and acetonitrile stretching vibrations predicted by DFT.

AUTHOR INFORMATION

Corresponding Author

* Dr Manja Kubeil, m.kubeil@hzdr.de.

Present Addresses

† Institute of Radiopharmaceutical Cancer Research, Helmholtz - Zentrum Dresden - Rossendorf, Bautzner Landstraße 400, D-01328, Dresden, Germany.

Notes

The authors declare no competing financial interest.

Author Contributions

The manuscript was written through contributions of all authors. All authors have given approval to the final version of the manuscript.

ACKNOWLEDGMENT

MK was supported by a Marie Curie International Outgoing Fellowship from the European Union's Seventh Framework Programme for research, technological development and demonstration under grant agreement no. 627113. RRV thanks the Monash Warwick Alliance for their support and travel funding as part of the Monash University and the University of Warwick Joint PhD program. BRW and BG are supported by ARC Future Fellowship grants FT120100926 and FT130100838, respectively. We acknowledge Mr Finlay Shanks for instrumental support within the Centre for Biospectroscopy at Monash University, and the Monash Campus Cluster at the Monash e-Research Centre for computational facilities.

ABBREVIATIONS

CORM, carbon monoxide releasing molecules; TD-DFT, time-dependent density functional theory; MCR-ALS, Multivariate Curve Resolution – Alternating Least Squares; FTIR, Fourier transform infrared spectroscopy.

REFERENCES

1. Mann, B. E., CO-Releasing Molecules: A Personal View. *Organometallics* **2012,** *31*, 5728-5735.

2. Johnson, T. R.; Mann, B. E.; Clark, J. E.; Foresti, R.; Colin J. Green; Motterlini, R., Metal Carbonyls: A New Class of Pharmaceuticals? *Angew. Chem. Int. Ed.* **2003,** *42*, 3722 – 3729.

3. Motterlini, R.; Otterbein, L. E., The therapeutic potential of carbon monoxide. *Nat. Rev. Drug Discov.* **2010,** *9*, 728-743.

4. Inaba, H.; Fujita, K.; Ueno, T., Design of biomaterials for intracellular delivery of carbon monoxide. *Biomater. Sci.* **2015,** *3*, 1423–1438.

5. Marhenke, J.; Trevino, K.; Works, C., The chemistry, biology and design of photochemical CO releasing molecules and the efforts to detect CO for biological applications. *Coord. Chem. Rev.* **2016,** *306*, 533-543.

6. Schatzschneider, U., Novel lead structures and activation mechanisms for CO-releasing molecules (CORMs). *Br. J. Pharmacol.* **2015,** *172*, 1638-1650.

7. Zobi, F., CO and CO-releasing molecules in medicinal chemistry. *Future Med. Chem.* **2013,** *5*, 175-188.

8. Garcia-Gallego, S.; Bernardes, G. J. L., Carbon-Monoxide-Releasing Molecules for the Delivery of Therapeutic CO In Vivo. *Angew. Chem. Int. Ed.* **2014,** *53*, 9712 – 9721.

9. Chakraborty, I.; Carrington, S. J.; Mascharak, P. K., Design Strategies To Improve the Sensitivity of Photoactive Metal Carbonyl Complexes (photoCORMs) to Visible Light and Their Potential as CO-Donors to Biological Targets. *Acc. Chem. Res.* **2014,** *47*, 2603−2611.

10. Romao, C. C.; Blaettler, W. A.; Seixas, J. D.; Bernardes, G. J. L., Developing drug molecules for therapy with carbon monoxide. *Chem. Soc. Rev.* **2012,** *41*, 3571-3583.

11. Heinemann, S. H.; Hoshi, T.; Westerhausend, M.; Schiller, A., Carbon monoxide – physiology, detection and controlled release. *Chem. Commun.* **2104,** *50*, 3644-3660.

12. Ward, J. S.; Bray, J. T. W.; Aucott, B. J.; Wagner, C.; Pridmore, N. E.; Whitwood, A. C.; Moir, J. W. B.; Lynam, J. M.; Fairlamb, I. J. S., Photoactivated Functionizable Tetracarbonyl(phenylpyridine)manganese(I) Complexes as COReleasing Molecules: A Direct Suzuki–Miyaura Cross-Coupling on a Thermally Stable CO-RM. *Eur. J. Inorg. Chem.* **2016**, 5044–5051.

13. Ward, J. S.; Lynam, J. M.; Moir, J. W. B.; Sanin, D. E.; Mountford, A. P.; Fairlamb, I. J. S., A therapeutically viable photo-activated manganese-based CO-releasing molecule (photo-CO-RM). *Dalton Trans.* **2012,** *41*, 10514–10517.

14. Chakraborty, I.; Carrington, S. J.; Mascharak, P. K., Photodelivery of CO by Designed PhotoCORMs: Correlation between Absorption in the Visible Region and Metal–CO Bond Labilization in Carbonyl Complexes. *ChemMedChem* **2014,** *9*, 1266 – 1274.

15. Rimmer, R. D.; Pierri, A. E.; Ford, P. C., Photochemically activated carbon monoxide release for biological targets. Toward developing air-stable photoCORMs labilized by visible light. *Coord. Chem. Rev.* **2012,** *256*, 1509– 1519.

16. Wright, M. A.; Wright, J. A., PhotoCORMs: CO release moves into the visible. *Dalton Trans.* **2016,** *45*, 6801-6811.

17. Ward, J. S.; Lynam, J. M.; Moir, J.; Fairlamb, I. J. S., Visible-Light-Induced CO Release from a Therapeutically Viable Tryptophan-Derived Manganese(I) Carbonyl (TryptoCORM) Exhibiting Potent Inhibition against E. coli. *Chem. Eur. J.* **2014,** *20*, 15061 – 15068.

18. Bonnet, S., Shifting the Light Activation of Metallodrugs to the Red and Near-Infrared Region in Anticancer Phototherapy. *Comments Inorg. Chem.* **2015,** *35*, 1-35.

19. Pierri, A. E.; Huang, P.-J.; Garcia, J. V.; Stanfill, J. G.; Chui, M.; Wu, G.; Zheng, N.; Ford, P. C., A photoCORM nanocarrier for CO release using NIR light. *Chem. Commun.* **2015,** *51*, 2072-2075.

20. Collomb-Dunand-Sauthier, M.; Deronzier, A.; Ziessel, R., Photochemical reactivity of $[Ru^{II}(L)(CO)_2Cl_2]$ and [Me,N] $[Ru^{II}(L)(CO)Cl_3]$ (L = 2,2'-bipyridine or 4,4'-di(isopropoxycarbonyl)-2,2'-bipyridine) in CH_3CN and the redox properties of the resulting new complexes. *J. Organomet. Chem.* **1993,** *444*, 191-198.

21. Eskelinen, E.; Haukka, M.; Venäläinen, T.; Pakkanen, T. A.; Wasberg, M.; Chardon-Noblat, S.; Deronzier, A., Light-Induced Decarbonylation, Solvolysis, and Isomerization of $Ru(L)(CO)_2Cl_2$ (L = 2,2'-Bipyridine and 4,4'-Dimethyl-2,2'-bipyridine) in Acetonitrile. *Organometallics* **2000,** *19*, 163-169.

22. Eskelinen, E.; Luukkanen, S.; Haukka, M.; Ahlgrén, M.; Pakkanen, T. A., Redox and photochemical behaviour of ruthenium(II) complexes with H_2dcbpy ligand (H_2dcbpy= 2,2'-bipyridine-4,4'-dicarboxylic acid). *J. Chem. Soc., Dalton Trans.* **2000**, 2745–2752.

23. Gabrielsson, A.; Zális, S.; Matousek, P.; Towrie, M.; Vlcek, A. J., Ultrafast Photochemical Dissociation of an Equatorial CO Ligand from trans(*X*,*X*)-$[Ru(X)_2(CO)_2(bpy)]$ (X = Cl, Br, I): A Picosecond Time-Resolved Infrared Spectroscopic and DFT Computational Study. *Inorg. Chem.* **2004,** *43*, 7380-7388.

24. Spiccia, L.; Deacon, G. B.; Kepert, C. M., Synthetic routes to homoleptic and heteroleptic ruthenium(II) complexes incorporating bidentate imine ligands. *Coord. Chem. Rev.* **2004,** *248*, 1329-1341.

25. Anderson, P. A.; Deacon, G. B.; Haarmann, K. H.; Keene, F. R.; Meyer, T. J.; Reitsma, D. A.; Skelton, B. W.; Strouse, G. F.; Thomas, N. C.; Treadway, J. A.; White, A. H., Designed Synthesis of Mononuclear Tris(heteroleptic) Ruthenium Complexes Containing Bidentate Polypyridyl Ligands. *Inorg. Chem.* **1995,** *34*, 6145-6157.

26. Badger, G.; Sasse, W. H. F., Synthetic Applications of Activated Metal Catalysts. Part II. The Formation of Heterocyclic Diaryls. *J. Chem. Soc.* **1956**, 616-620.

27. Strouse, G. F.; Andenon, P. A.; Schoonover, J. R.; Meyer, T. J.; Keene, F. R., Synthesis of Polypyridyl Complexes of Ruthenium(II) Containing Three Different Bidentate Ligands. *Inorg. Chem.* **1992,** *31*, 3004-3006.

28. Nickita, N.; Belousoff, M. J.; Bhatt, A. I.; Bond, A. M.; Deacon, G. B.; Gasser, G.; Spiccia, L., Synthesis, Structure, Spectroscopic Properties, and Electrochemical Oxidation of Ruthenium(II) Complexes Incorporating Monocarboxylate Bipyridine Ligands. *Inorg. Chem.* **2007,** *46* (21), 8638-8651.

29. Jaumot, J.; Gargallo, R.; Juan, A. d.; Tauler, R., A graphical user-friendly interface for MCR-ALS: a new tool for multivariate curve resolution in MATLAB. *Chemometrics Intell. Lab. Syst.* **2005,** *76*, 101–110.

30. Tauler, R.; Smilde, A.; Kowalski, B., Selectivity, Local Rank, Three-Way Data Analysis and Ambiguity in Multivariate Curve Resolution. *J. Chemom.* **1995,** *9*, 31-58.

31. Frisch, M. J. T., G. W.; Schlegel, H. B.; Scuseria, G. E.; Robb, M. A.; Cheeseman, J. R.; Scalmani, G.; Barone, V.; Mennucci, B.; Petersson, G. A.; Nakatsuji, H.; Caricato, M.; Li, X.; Hratchian, H. P.; Izmaylov, A. F.; Bloino, J.; Zheng, G.; Sonnenberg, J. L.; Hada, M.; Ehara, M.; Toyota, K.; Fukuda, R.; Hasegawa, J.; Ishida, M.; Nakajima, T.; Honda, Y.; Kitao, O.; Nakai, H.; Vreven, T.; Montgomery, J. A., Jr.; Peralta, J. E.; Ogliaro, F.; Bearpark, M.; Heyd, J. J.; Brothers,

E.; Kudin, K. N.; Staroverov, V. N.; Kobayashi, R.; Normand, J.; Raghavachari, K.; Rendell, A.; Burant, J. C.; Iyengar, S. S.; Tomasi, J.; Cossi, M.; Rega, N.; Millam, M. J.; Klene, M.; Knox, J. E.; Cross, J. B.; Bakken, V.; Adamo, C.; Jaramillo, J.; Gomperts, R.; Stratmann, R. E.; Yazyev, O.; Austin, A. J.; Cammi, R.; Pomelli, C.; Ochterski, J. W.; Martin, R. L.; Morokuma, K.; Zakrzewski, V. G.; Voth, G. A.; Salvador, P.; Dannenberg, J. J.; Dapprich, S.; Daniels, A. D.; Farkas, Ö.; Foresman, J. B.; Ortiz, J. V.; Cioslowski, J.; Fox, D.J. *Gaussian 09 (Revision A.02)*, Gaussian, Inc.: Wallingford CT, 2009.

32. Peterson, K. A.; Figgen, D.; Dolg, M.; Stoll, H., Energy-consistent relativistic pseudopotentials and correlation consistent basis sets for the 4d elements Y–Pd. *J. Phys. Chem. A* **2007,** *126*, 124101.

33. Barone, V.; Cossi, M., Quantum Calculation of Molecular Energies and Energy Gradients in Solution by a Conductor Solvent Model. *J. Phys. Chem. A* **1998,** *102*, 1995-2001.

34. Cossi, M.; Rega, N.; Scalmani, G.; Barone, V., Energies, structures, and electronic properties of molecules in solution with the C-PCM solvation model. *J. Comput. Chem.* **2003,** *24*, 669-81.

35. Tomasi, J.; Mennucci, B.; Cammi, R., Quantum Mechanical Continuum Solvation Models. *Chem. Rev.* **2005,** *105*, 2999-3094.

36. Homanen, P.; Haukka, M.; Luukkanen, S.; Ahlgrén, M.; Pakkanen, T. A., Selective Formation of cis(X)- and trans(X)-Ru(dmbpy)$(CO)_2X_2$ Complexes (X = Cl, Br, I, SCN) from

Monomeric and Dimeric Ru–mono(dmbpy) Carbonyl Complexes (Dmbpy = 4,4′-Dimethyl-2,2′-bipyridine). *Eur. J. Inorg. Chem.* **1999,** *1999*, 101-106.

37. Bischof, C.; Joshi, T.; Dimri, A.; Spiccia, L.; Schatzschneider, U., Synthesis, Spectroscopic Properties, and Photoinduced CO-Release Studies of Functionalized Ruthenium(II) Polypyridyl Complexes: Versatile Building Blocks for Development of CORM−Peptide Nucleic Acid Bioconjugates. *Inorg. Chem.* **2013,** *52*, 9297-9308.

38. Dennington, R. K., T.; Millam, J. *GaussView (Version 5)*, Semichem Inc.: Shawnee Mission, KS, 2009.

39. Balducci, G.; Iengo, E.; Demitri, N.; Alessio, E., New Insight into a Deceptively Simple Reaction: The Coordination of bpy to Ru^{II}–Carbonyl Precursors – The Central Role of the fac-$[Ru(bpy)Cl(CO)_3]^+$ Intermediate and the Chloride Rebound Mechanism. *Eur. J. Inorg. Chem.* **2015**, 4296-4311.

40. Black, D. S. C.; Deacon, G. B.; Thomas, N. C., Ruthenium Carbonyl Complexes. Synthesis of $[Ru(CO)_2(bidentate)_2]^{2+}$ Complexes. *Aust. J. Chem.* **1982,** *35*, 2445-2453.

41. Haukka, M.; Kiviaho, J.; Ahlgrh, M.; Pakkanen, T. A., Studies on Catalytically Active Ruthenium Carbonyl Bipyridine Systems. Synthesis and Structural Characterization of $[Ru(bpy)(CO)_2Cl_2]$, $[Ru(bpy)(CO)_2Cl(C(O)OCH_3)]$, $[Ru(bpy)(CO)_2Cl]_2$, and $[Ru(bpy)(CO)_2ClH]$ (bpy = 2,2'-Bipyridine). *Organometallics* **1995,** *14*, 825-833.

42. Kuramochi, Y.; Fukaya, K.; Yoshida, M.; Ishida, H., *trans*-(Cl)-[Ru(5,5'-diamide-2,2'-bipyridine)$(CO)_2Cl_2$]: Synthesis, Structure, and Photocatalytic CO_2 Reduction Activity. *Chem. Eur. J.* **2015,** *21*, 10049-10060.

43. Moreno, M. A.; Matti, H.; Kallinen, M.; Pakkanen, T. A., Reactions of $[Ru(CO)_3Cl_2]_2$ with aromatic nitrogen donor ligands in alcoholic media. *Appl. Organometal. Chem.* **2006,** *20*, 51-69.

44. Göttle, A. J.; Alary, F.; Boggio-Pasqua, M.; Dixon, I. M.; Heully, J.-L.; Bahreman, A.; Askes, S. H. C.; Bonnet, S., Pivotal Role of a Pentacoordinate 3MC State on the Photocleavage Efficiency of a Thioether Ligand in Ruthenium(II) Complexes: A Theoretical Mechanistic Study. *Inorg. Chem.* **2016,** *55*, 4448-4456.

45. Hehre, W. J.; Radom, L.; Schleyer, P. v. R.; Pople, J. A., *Ab initio molecular orbital theory*. New York : Wiley: New York, 1986.

46. Scott, A. P.; Radom, L., Harmonic Vibrational Frequencies: An Evaluation of Hartree−Fock, Møller−Plesset, Quadratic Configuration Interaction, Density Functional Theory, and Semiempirical Scale Factors. *J. Phys. Chem.* **1996,** *100*, 16502-16513.

Table of Contents Synopsis and Graphic

UV light-triggered CORMs: The mechanism and kinetics of CO release from three Ru(II) bipyridine carbonyl complexes with different electronic properties have been elucidated using a combination of UV-Vis absorbance and FTIR spectroscopies, multivariate curve resolution analysis and density functional theory calculations.